Chapter 6. Fatigue Analysis of GNP and Aligned Fe_3O_4-GNP Epoxy Nanocomposite

6.1. Introduction

This study analyzes the cyclic fatigue of nanocomposites reinforced with GNP and aligned Fe_3O_4-GNP nanoparticles. The main objective is to investigate the influence of Fe_3O_4-GNP alignment on cyclic fatigue. A comparative study between GNP and aligned Fe_3O_4-GNP nanocomposites is conducted. No previous research [3–11,13–17,19–44] specifically focusing on this study has been found in the literature. The study aims to achieve the following:

- Fabricate well-dispersed GNP and Fe_3O_4-GNP reinforced nanocomposites, along with aligned Fe_3O_4-GNP nanocomposites using optimized alignment parameters.
- Examine the effects of Fe_3O_4-GNP alignment and nanoparticle weight percentage on threshold fatigue properties (ΔK_{th} and ΔG_{th}), fatigue crack growth rate, and the constants of the Paris law.
- Analyze stereo zoom optical and atomic force microscopy (AFM) images of fractured surfaces to investigate the underlying mechanisms influencing fatigue crack growth rate.
- Conduct a comprehensive analysis of fracture surface roughness parameters to understand FCGR resistance and energy dissipation mechanisms.

Overall, this study aims to provide new insights into the cyclic fatigue behavior of nanocomposites reinforced with GNP and aligned Fe_3O_4-GNP nanoparticles, filling the existing research gap in the literature.

6.2.Experimental procedure

6.2.1. Materials and specimen preparation the nanocomposites

As mentioned in section 4.2.1 to 4.2.3.

A mild steel pattern has been produced with a V-shaped notch having a width of 1.6 mm and a tip radius of 0.20 mm to fabricate the mould cavity that accurately matches the impression of the CT specimen following ASTM 5045-99[35], shown in **Fig. 5.3**. Moreover, a knife-edge

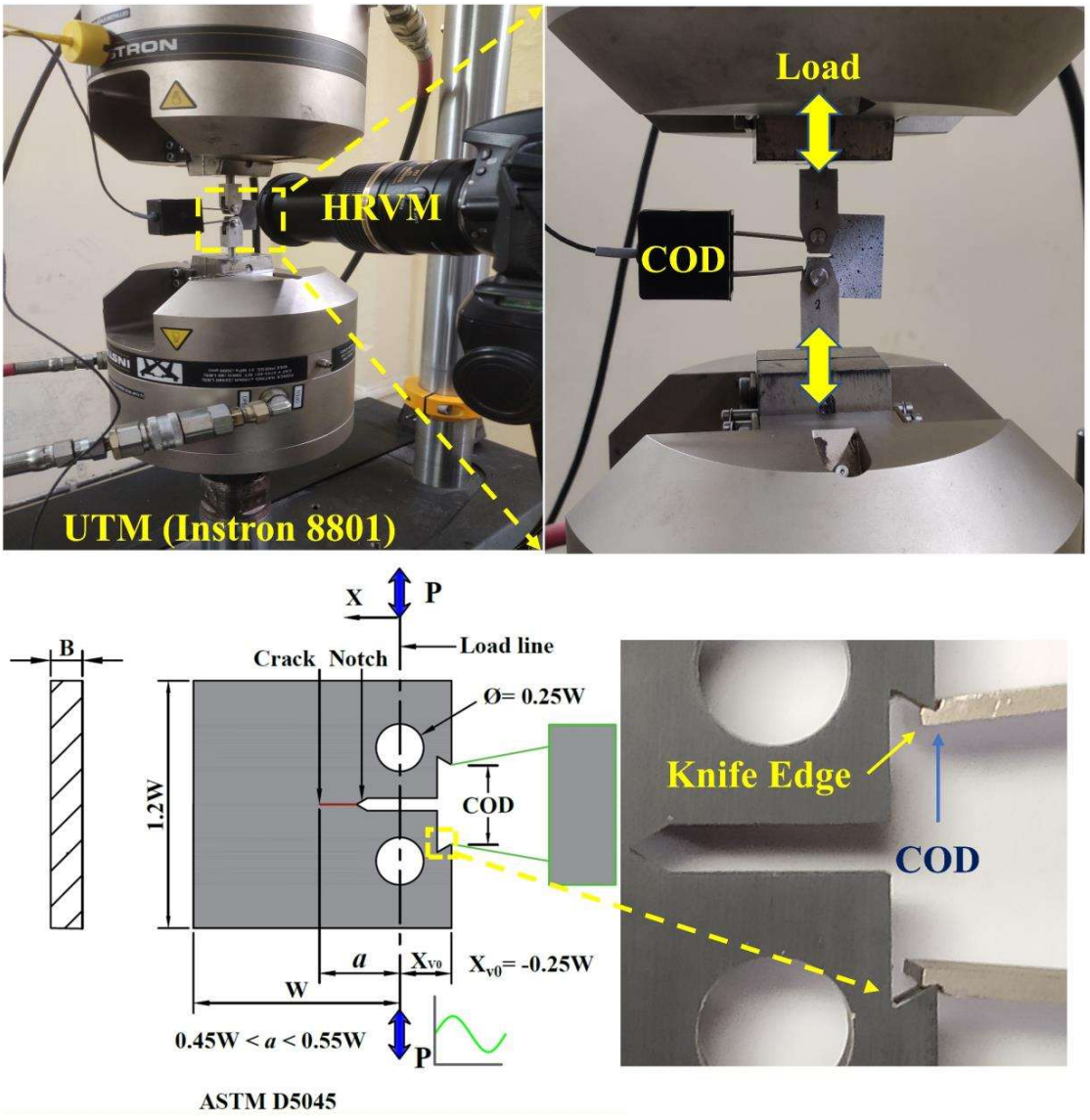

Fig. 6.1. Illustrates the experimental arrangement, with a CT specimen employed according to ASTM standards for fracture testing and also attachment of the COD to the CT specimen through the implementation of a knife-edge configuration.

geometry has been created at the notch's opening mouth to facilitate the compatible attachment of the COD. The pattern has been machined using wire Electrical Discharge Machining (EDM) on the Expresscut Series-EX 4032C machine with a wire diameter of 0.20 mm. A precise impression has been obtained by cold-casting in RTV silicon rubber by the pattern. The final mould obtained by this process has exact dimensions for accurately casting the CT specimen.

In the last chapter, we have conducted tensile and fracture toughness tests on neat epoxy and a nanocomposite reinforced with GNP and aligned Fe_3O_4-GNP nanoparticles for different wt% in accordance with ASTM D638 and ASTM D5045-99 standards [196,200]. These tests have been performed at room temperature (30°C) using appropriate technical procedures. The outcome of these tests has been compiled and presented in Table 5.1.

6.2.2. Cyclic fatigue and FCGR test

The compact tension (CT) specimen was employed to perform cyclic fatigue testing. The test protocol was rigorously executed per the guidelines outlined in ASTM D5045-99[35]. The testing was conducted at a frequency of 5 Hz using the Instron 8801 servo hydraulic fatigue tester. Before proceeding with testing to eliminate the notch effect, it is imperative to create an initial pre-crack in the specimen by delicately tapping a new cooled razor blade over a molded starter notch tip. This process ensures the initiation of a sharp crack, referred to as 'a_0,' with a length falling within the range of 0.45 W and 0.55 W. It involved the application of cyclic loading through constant load amplitude (ΔP) sinusoidal waveform, commonly known as the K-increasing test procedure (**Fig. 6.3)**. The load ratio, $R = P_{min}/P_{max}$, was maintained at 0.1 under tension-tension mode and load control to maintain consistency. Load range mapping ($\Delta P = P_{max} - P_{min}$) was carried out to ensure the accuracy of the results. For precise force application of less than 100 N, a 2kN load cell (Dynacell™, Catalogue Number 2527-129) with an accuracy of 0.5% was employed.

The COD of CT specimens was evaluated using an Instron Model 2670-116 (Output:-2 to 4 mV/V nominal, Output Sensitivity;-2.5 mV/V +1% -3% at 30 °C, Electrical calibration accuracy:- ± 0.1 % full-scale deflection) clip-gage affixed to the specimen at the crack mouth via inbuilt knife edges at position $X_{V0} = -0.25W$ and aligned parallel to the notch surface as details in ASTM E647 [224]. Data acquisition was done using Instron Fast Track Max software while optical crack length measurements were taken on the front face of the CT specimen using a high-resolution video monitoring (HRVM) system of Nikon with Micro Lens (depicted in **Fig. 5.3**). The accuracy of crack length measurement is contingent upon the precise calibration of the COD for the relevant specimen, which is carried out according to the methodology prescribed in reference [203,225–228]. With the compliance approach, the expression of crack length, *a*, (for $0.2 \leq a/W \leq 0.975$) defined as:

$$\frac{a}{W} = C_0 + C_1 U_x + C_2 U_x^2 + C_3 U_x^3 + C_4 U_x^4 + C_5 U_x^5, \tag{6.1}$$

where, the constants are:

$$\begin{aligned} &C_0 = 1.001, \quad C_2 = 18.46, \quad C_4 = 1214.9, \\ &C_1 = -4.6695, \quad C_3 = -236.82, \quad C_5 = -2143.6 \end{aligned} \tag{6.2}$$

And variable is:

$$U_x = \left\{ 1 + \left[BE \frac{COD}{P} \right]^{\frac{1}{2}} \right\}^{-1} \tag{6.3}$$

The lengths of cracks were assessed at intervals of 100 cycles and verified through optical means utilizing the HRVM system. While, FCGR initially progresses slowly but accelerates as the crack size increases, resulting in an increase in da/dN. ASTM E647 [224] standard recommends using the incremental polynomial technique to determine the da/dN parameter. The initial value for P_{max} has been determined as $\Delta K = K_{IC}/2$, where the K_{IC} is the stress intensity factor of quasi static fracture test and has been noted in Table 5.1 for different wt %. While, the ΔK during crack propagation has expressed as:

$$\Delta K = \frac{\Delta P}{B\sqrt{W}} \frac{2+\alpha}{(1-\alpha)^{3/2}} (0.886 + 4.64\alpha - 13.32\alpha^2 + 14.72\alpha^3 - 5.6\alpha^4) \quad (6.4)$$

where, $\alpha = a/W$ has related to the sample's shape. ΔK_{th} measures a material's capacity to withstand subcritical crack propagation, particularly when the crack grows by approximately 2 μm over the course of 10^5 cycles. The experimental evaluation of ΔK_{th} has entailed a thorough and meticulous process, which has been comprehensively outlined in a flowchart (**Fig. 6.2**). This process has necessitated 15-16 hours (~2,50,000 cycles for a specimen) of dedicated usage with multiple samples to ensure the accuracy and validity of results. Subsequently, the calculation of ΔG_I and ΔG_{th} was carried out based on the ΔK_I and ΔK_{th} values, utilizing the following relation:

$$G_{IC} = \frac{(1-\nu^2)K_{IC}^2}{E} \quad (6.5)$$

A minimum of five specimens for each nanocomposite type were subjected to testing, following which the mean value was computed and documented. This approach has ensured that the data collected has been both reliable and statistically significant.

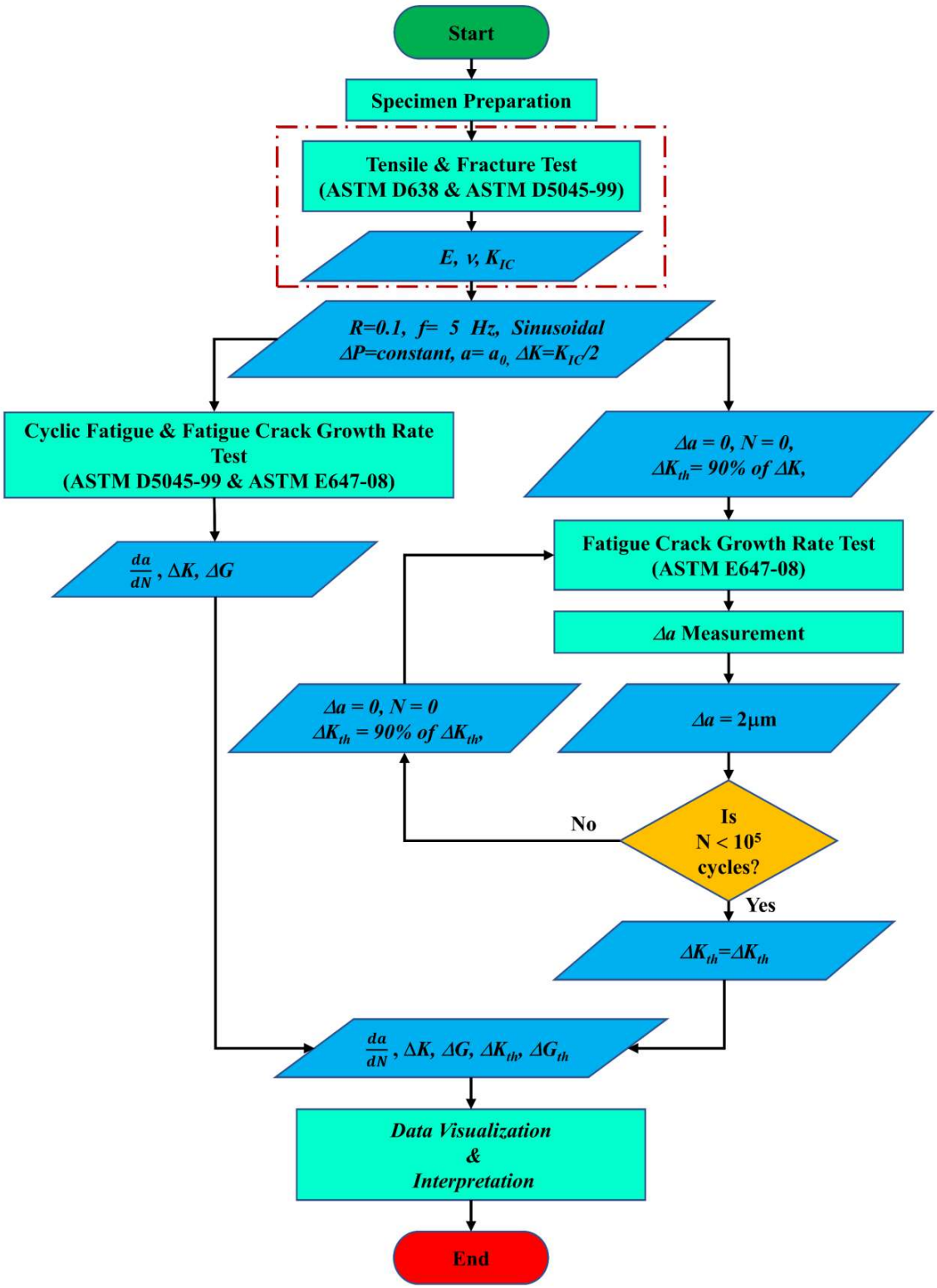

Fig. 6.2. Illustrates an algorithm flowchart that explicitly outlines each step involved in the computation of fatigue crack growth parameters.

6.2.3. Fatigue fracture surface analysis

We used a stereo zoom optical microscope (Model RSM 9, IS300, 3.0MP) from Radical Scientific to examine fractured surfaces. This helped us understand the deformation and failure mechanisms caused by nanoparticles during fatigue crack growth. The microscope allowed us to qualitatively assess the surface texture and observe how cracks propagate. Additionally, we employed atomic force microscopy (AFM) with a scanning probe microscope (NTEGRA Prima, NT-MDT Service & Logistics Ltd.) to determine post-fracture surface roughness parameters. Using the tapping technique, we scanned 10 μm x 10 μm spots near crack points and analyzed the resulting micrographs with Gwyddion software, a free and open-source tool for scanning probe microscopy data visualization and analysis.

6.3. Result

The fatigue process encompasses the initiation and propagation of microcracks, which can arise from macroscopic material discontinuities or inclusions within the material. In the case of composite materials, the reinforced second phase material often serves as the principal site for initiating fatigue cracks. Additionally, the size and shape of preexisting flaws significantly influence the initiation and subsequent growth of cracks during cyclic fatigue loading. These factors collectively play a critical role in determining the behavior and progression of fatigue cracks. The persistent concern surrounding fatigue damage in a wide range of polymers and structures under varying stress states has prompted our comprehensive research efforts. To address this critical issue, we have conducted exhaustive fatigue experiments, specifically focusing on cyclic tension-tension testing of CT specimen inbuilt crack attached with COD of epoxy, GNP epoxy, and Aligned Fe_3O_4-GNP epoxy nanocomposites. The primary objective of these experiments was to thoroughly investigate and analyze the intrinsic and interfacial fatigue behavior displayed by these materials.

6.3.1. Cyclic fatigue loading and its response.

During the compact tension fatigue test, the values of the applied load P and the response of the COD have been meticulously recorded for a representative cycle involving loading and unloading **Fig. 6.3**. These recorded values provide crucial data to analyze and evaluate the performance and durability of the material under cyclic loading conditions.

During the progressive growth of the crack length, there has been a consistent increase in the values of COD and other relevant parameters observed throughout subsequent overload cycles. **Fig. 6.4** presents a comprehensive plot showcasing the measured hysteresis variations between *P* and COD during the tests under discussion. For two representative F=f(COD) hysteresis loops, the loading and unloading half-cycles of subsequent levels of constant-amplitude loads have been meticulously recorded. The decline in slopes of these loops during subsequent load cycles has been characterized and directly utilized in compliance computation. The area enclosed by these hysteresis loops has exhibited an incremental rise with the number of cycles, serving as an indicator of crack length expansion and the accompanying dissipation of strain energy. The hysteresis loss measurements are vital for evaluating polymers' resistance to crack initiation and crazing during fatigue crack growth. They quantitatively assess energy dissipation and internal friction during cyclic loading, offering insights into crack initiation and resistance to crazing. These measurements contribute to characterizing polymer durability and reliability under fatigue crack growth, advancing materials engineering and the design of robust structures. The figure provides a detailed analysis of the cyclic behavior exhibited by the nanocomposite, showcasing the relationship between the applied load and the corresponding COD response. This investigation offers valuable insights into the material's performance and behavior under cyclic loading conditions. These factors collectively govern the rate of fatigue crack growth.

Fatigue cracks exhibit growth patterns with increasing load cycles under specific conditions. In this study, an initial crack underwent pure mode I loading, propagating along its original path (refer to **Fig. 6.1**). The crack growth rate was quantified by measuring the change in crack length *(Δa)* per load cycle change (ΔN) within a defined time interval. By extrapolating to ΔN approaching zero, the crack growth rate was determined as the slope *(da/dN*) of the crack length plotted against the load cycle curve (**Fig. 6.5)**.

Fig. 6.6 helps us understand how applied loading cycles, crack growth, and FCGR are connected. It gives us important information about how cracks growth rate. At low crack growth and higher cycle counts, the rate decreases due to factors like crack bridging, bifurcation, twisting and tilting of cracks, impeding growth and mitigating fatigue damage. Conversely, as crack growth intensifies and cycle counts decrease, the rate increases, indicating accelerated propagation in a deteriorating material with reduced resistance. These findings offer valuable information on the FCGR and insights into crack stability. Stable crack growth demonstrates a gradual increase, reflecting predictability and control, while the unstable crack region exhibits an exponential surge, signifying rapid and unpredictable advancement with higher risk to structural integrity. In summary, the results in **Fig. 6.6** emphasize the intricate interplay between loading cycles, crack growth, and fatigue crack growth rate, enhancing our understanding of fatigue mechanisms and facilitating the development of effective strategies for fatigue life prediction and structural integrity assessment.

Under constant amplitude loads, crack propagation and growth rate accelerate with more load cycles. The applied load magnitude influences the behavior of the *a*-N curve, impacting the

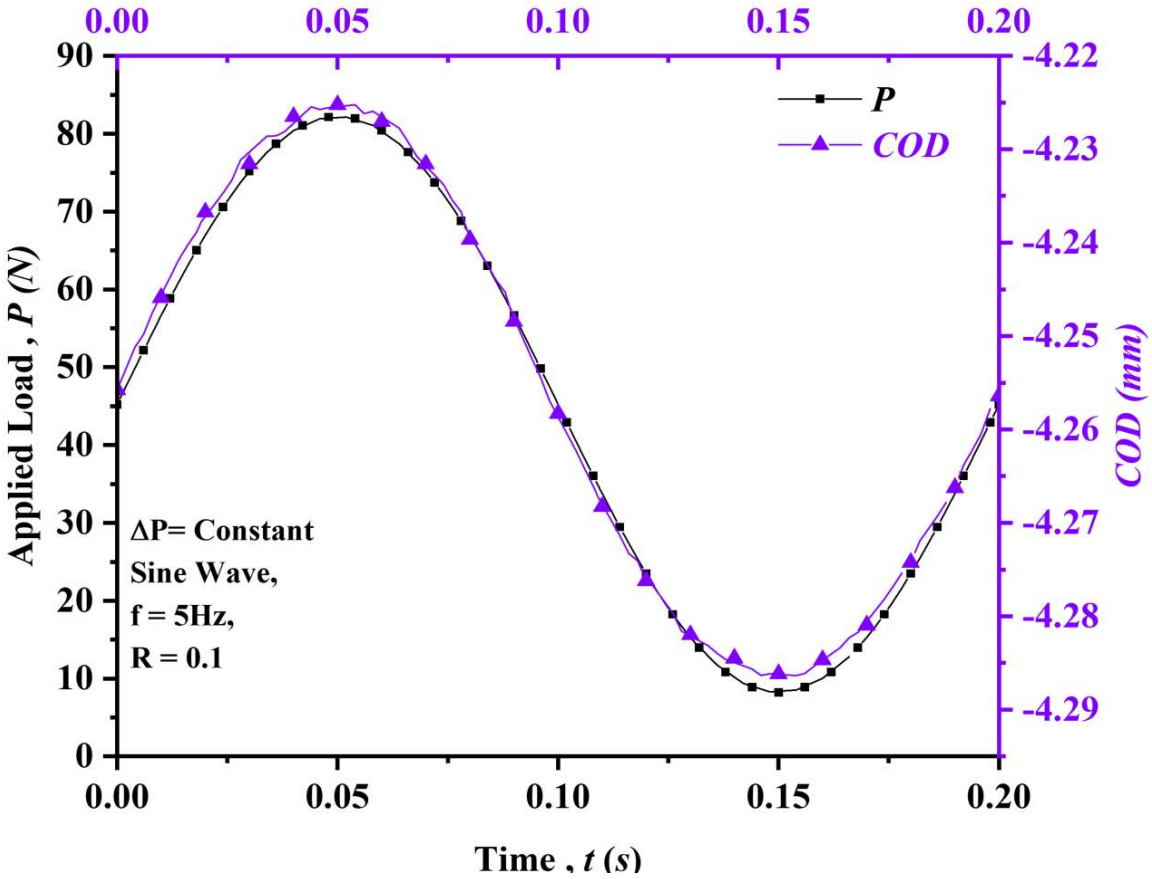

Fig. 6.3. Illustrates the COD response under the applied sinusoidal load for a typical cycle of a nanocomposite.

crack growth rate. Higher loads decrease the slope of hysteresis loops while increasing the area enclosed by them. These variations directly affect the crack growth rate, leading to elevated rates and unstable crack growth, particularly with shorter crack lengths[229]. The crack growth rate has been observed to be influenced by a range of factors, including material properties, thereby requiring experimental determination. The subsequent section delves into a comprehensive exploration of additional details pertaining to this phenomenon.

Fig. 6.7 and **Fig. 6.8** presents the fatigue performance analysis of the epoxy, GNP epoxy, and aligned Fe_3O_4-GNP epoxy nanocomposites. The logarithmic plots (Log-Log) depicted in the figure demonstrate the correlation between the FCGR *(da/dN)* and the stress intensity factor

range *(ΔK_I),* as well as the stress intensity factor range *(ΔG_I).* Notably, the data consistently aligns with the anticipated modified Paris law relationship[230,231].

$$\frac{da}{dN} = C(\Delta K)^m \; or \; \frac{da}{dN} = C'(\Delta G)^{m/2} \tag{6.6}$$

where m, C and C' are all the materials. The constants are obtained from the experiments and summarized in theTable 6.1. The constants depend on testing parameters such as moisture, temperature, frequency, and stress ratio. Further elaboration on these constants is provided in the subsequent sections.

6.3.2. The impact of nanoparticles on thresholds for fatigue crack growth, ΔK_{th} and ΔG_{th}

The findings presented in **Fig. 6.7** and **Fig. 6.8** illustrate the typical results obtained for the epoxy, GNP epoxy, and aligned Fe_3O_4-GNP epoxy. This analysis has revealed several noteworthy observations. Firstly, a linear correlation between the logarithmic FCGR (da/dN) and the logarithmic range of applied stress-intensity factor (ΔK_{th}) and strain energy release rate), (ΔG_{th}) as per the well-established 'Paris Law region,' has been identified in both epoxy and

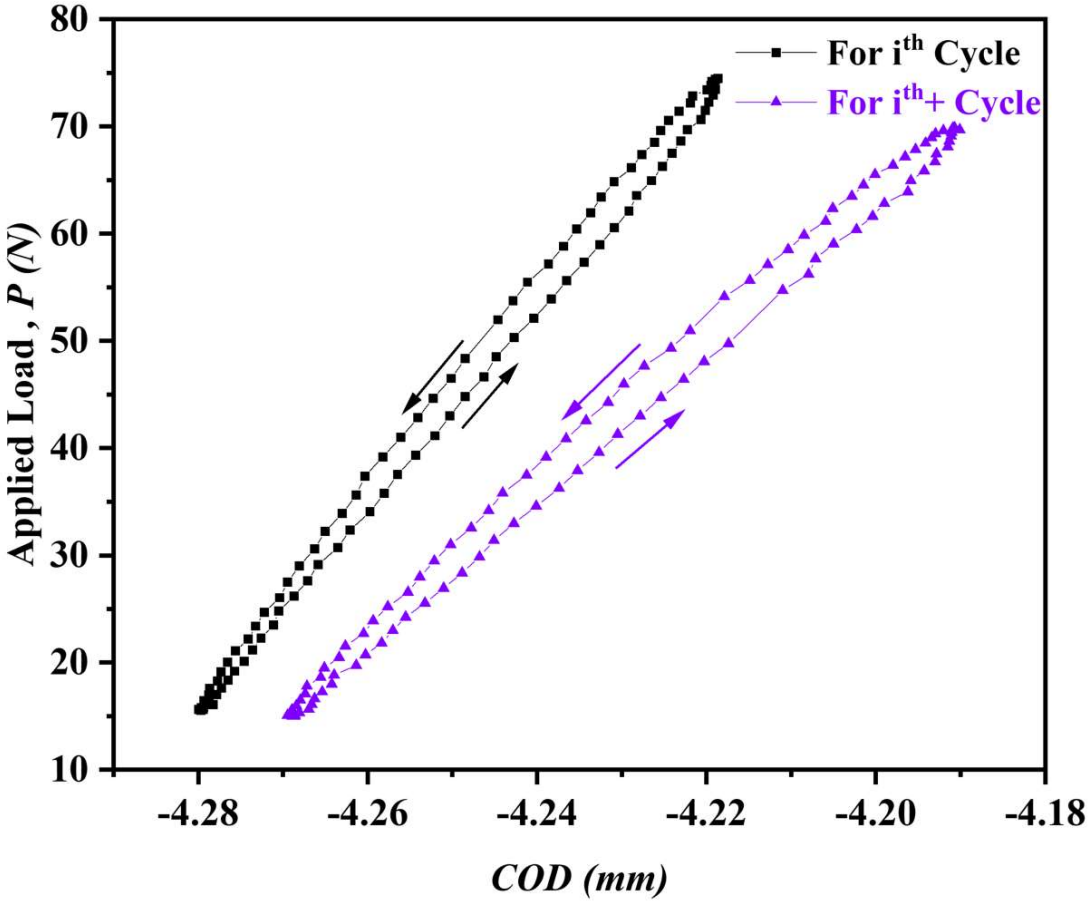

Fig. 6.4. show the hysteresis loops showcasing the relationship between the applied sinusoidal Load and the corresponding COD response of typical a nanocomposite during two representative progressive cycles .

nanocomposite materials. Secondly, a distinct 'threshold region' represented by (ΔK_{th} andΔG_{th}) has been observed, indicating the absence of cyclic-fatigue crack growth in both epoxy and nanocomposites below these threshold value. (ΔK_{th} andΔG_{th}) serves as a valuable parameter for

both material development and selection, as well as design engineering considerations. Thirdly, the incorporation of GNP nanoparticles and aligned Fe_3O_4-GNP nanoparticles has prominently improved the cyclic-fatigue properties of the epoxy polymer. The enhancement of ΔK_{th} becomes more pronounced with increasing weight percentage of nanoparticles, with the aligned Fe_3O_4-GNP nanoparticles playing a significant role in elevating the value of ΔK_{th} and ΔG_{th}.

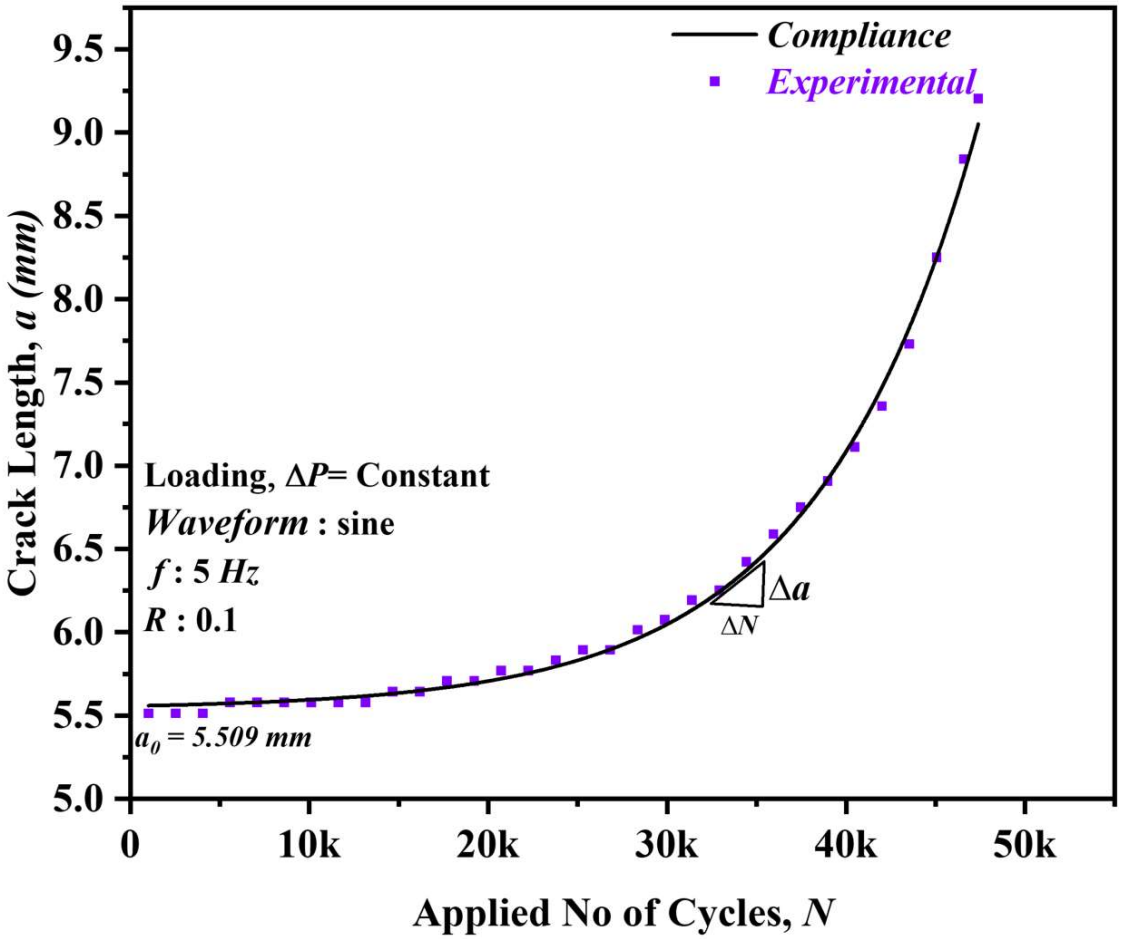

Fig. 6.5. Illustrates the COD response under the applied sinusoidal load for a typical cycle of a nanocomposite.

Table 6.1 provides a comprehensive summary of the thresholds, namely ΔK_{th}, ΔG_{th} , $\Delta K_{th}/K_{IC}$ and $\Delta G_{th}/G_{IC}$, for all nanocomposites. A clear trend is evident from the data, showing a consistent increase in the values of ΔK_{th} and ΔG_{th} as the toughness parameters, K_{IC} and G_{IC}, demonstrate higher values. This relationship becomes particularly pronounced with an

increased concentration of nanoparticles, and notably more so with the incorporation of aligned Fe_3O_4-GNP nanoparticles. The effectiveness of nanoparticles and the alignment of reinforcements in enhancing fatigue crack growth resistance has been convincingly demonstrated by analyzing the ratios of $\Delta K_{th}/K_{IC}$ and $\Delta G_{th}/G_{IC}$. Previous studies, cited as references [20,232–234], have consistently reported that the typical values for this ratio remain below around 35% of the critical value for static fracture parameters. **Fig. 6.9** and **Fig. 6.10** has depicted the variation in ΔK_{th} and ΔG_{th} as the wt% of both GNP and aligned Fe_3O_4-GNP nanoparticles increases. The results clearly indicate that an increased wt% leads to more pronounced enhancements, particularly observed in the aligned Fe_3O_4-GNP nanoparticles, which exhibit significantly improved ΔK_{th} and ΔG_{th} in comparison to randomly oriented GNP nanoparticles. Consequently, the incorporation of aligned Fe_3O_4-GNP nanoparticles has proven to be highly effective, as evidenced by measured values of $\Delta K_{th}/K_{IC}$ and $\Delta G_{th}/G_{IC}$ reaching up to 0.33 (as indicated in Table 6.1).

6.3.3. The influence of nanoparticles on the FCGR

The fatigue crack growth resistance has exhibited a consistent behavior across all nanocomposite materials at ΔK_{th} and ΔG_{th} [101]. This behavior shares similarities with

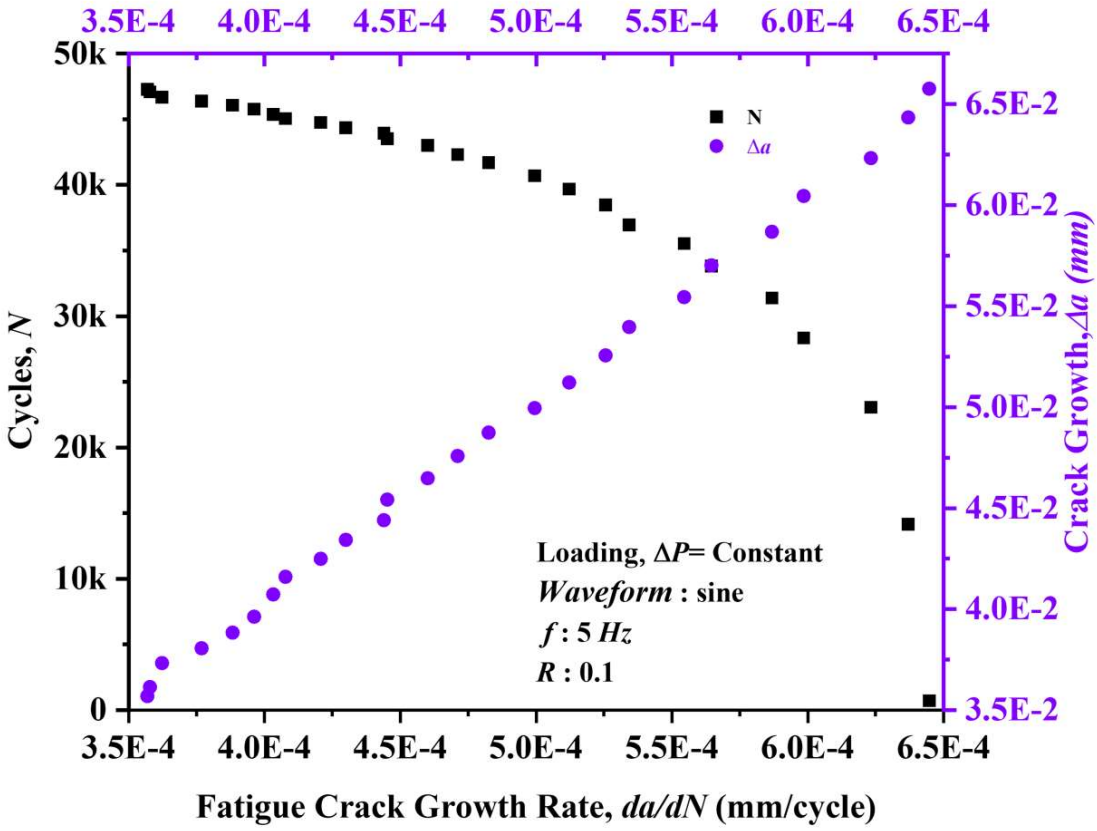

Fig. 6.6. Elucidates the fatigue crack growth rate at a specific number of cycles and corresponding crack growth for a typical a nanocomposite under the applied sinusoidal load.

observations made in epoxy composites incorporating rubber particles[15,101], where rubber cavitation and matrix dilation occur beyond specific ΔK_I and ΔG_I values, namely ΔK_{th} and ΔG_{th}. The identification of this transition point within our nanocomposites indicates the presence of distinct operating mechanisms below and above threshold values. Significantly, above this transition point, the influence of nanoparticles becomes evident, leading to considerable enhancements in reducing the fatigue crack growth rate: i) The FCGR has exhibited a comparatively slower increase with the applied stress intensity range in both the GNP and aligned Fe_3O_4-GNP epoxy nanocomposites, in contrast to the epoxy material. (ii) The GNP and

aligned Fe_3O_4-GNP epoxy nanocomposite has demonstrated superior resistance to fatigue crack growth, surpassing that of the epoxy material beyond the transition point. (iii) Aligned Fe_3O_4-GNP has exhibited a more pronounced deceleration of the FCGR when compared to randomly distributed nanoparticles, suggesting the presence of distinct and supplementary mechanisms during the crack propagation process.

The analysis of structural failure reveals the mechanisms behind crack initiation and progression in materials. Crack, arising from manufacturing or service, significantly impact structural integrity. These flaws gradually grow until reaching a critical size, leading to catastrophic failure. Parameters like ΔK_{th} and ΔG_{th} influence this failure process[235]. When the parameter ΔK_I exceeds the ΔK_{th}, or when ΔG_I surpasses ΔG_{th}, the flaw enters a stage of cyclic loading in accordance with the Paris law. The Paris law, represented by Eq. (6.6), describes the relationship between crack growth rate and stress intensity factor range, highlighting the role of cyclic loading in crack propagation. Under cyclic loading, the crack gradually enlarges until it reaches a critical dimension, leading to fracture at ΔK_I, represented by (1-R) K_{IC}[229]. This critical value represents the stress intensity factor required for crack propagation. The factors ΔK_{th} (or ΔG_{th}) and da/dN (FCGR) become essential in understanding and determining the fatigue life of a material. By analyzing the results presented in **Fig. 6.7** and **Fig. 6.8**, it becomes evident that the values of ΔK_{th} and ΔG_{th} for GNP and aligned Fe_3O_4-GNP are higher compared to those of epoxy. This indicates that the ΔK_{th} for crack growth is greater in the presence of GNP and aligned Fe_3O_4-GNP, suggesting improved resistance to crack propagation. Furthermore, the fatigue crack growth rate, da/dN, is lower for GNP and aligned Fe_3O_4-GNP compared to epoxy. This implies that the crack growth process is slower in the presence of these nanoparticles, further contributing to their enhanced fatigue performance.

Interestingly, aligned Fe_3O_4-GNP nanoparticles exhibit higher ΔK_{th} (or ΔG_{th}) values compared to GNP alone, indicating even greater resistance to crack growth. However, the da/dN rate for

aligned Fe_3O_4-GNP is slower compared to both GNP epoxy and epoxy alone. This suggests that while crack growth is effectively impeded in the presence of aligned Fe_3O_4-GNP, the actual rate of propagation is slower compared to the other materials. These findings highlight the superior fatigue crack growth resistance of GNP epoxy compared to epoxy alone, as evidenced by the higher ΔK_{th} (or ΔG_{th}) values and lower *da/dN* rate. Such resistance is directly correlated to increased fatigue lifetimes, indicating the improved durability and longevity of structures incorporating GNP epoxy. Remarkably, among the examined nanocomposites, aligned Fe_3O_4-GNP epoxy demonstrates the highest value of ΔK_{th} and ΔG_{th}. This suggests exceptional resistance to crack growth and enhanced fatigue performance, leading to extended fatigue lifetimes. These results underscore the potential of aligned Fe_3O_4-GNP epoxy as a promising material for applications where superior fatigue properties are paramount.

6.3.4. The impact of nanoparticles on the constant of the Paris law

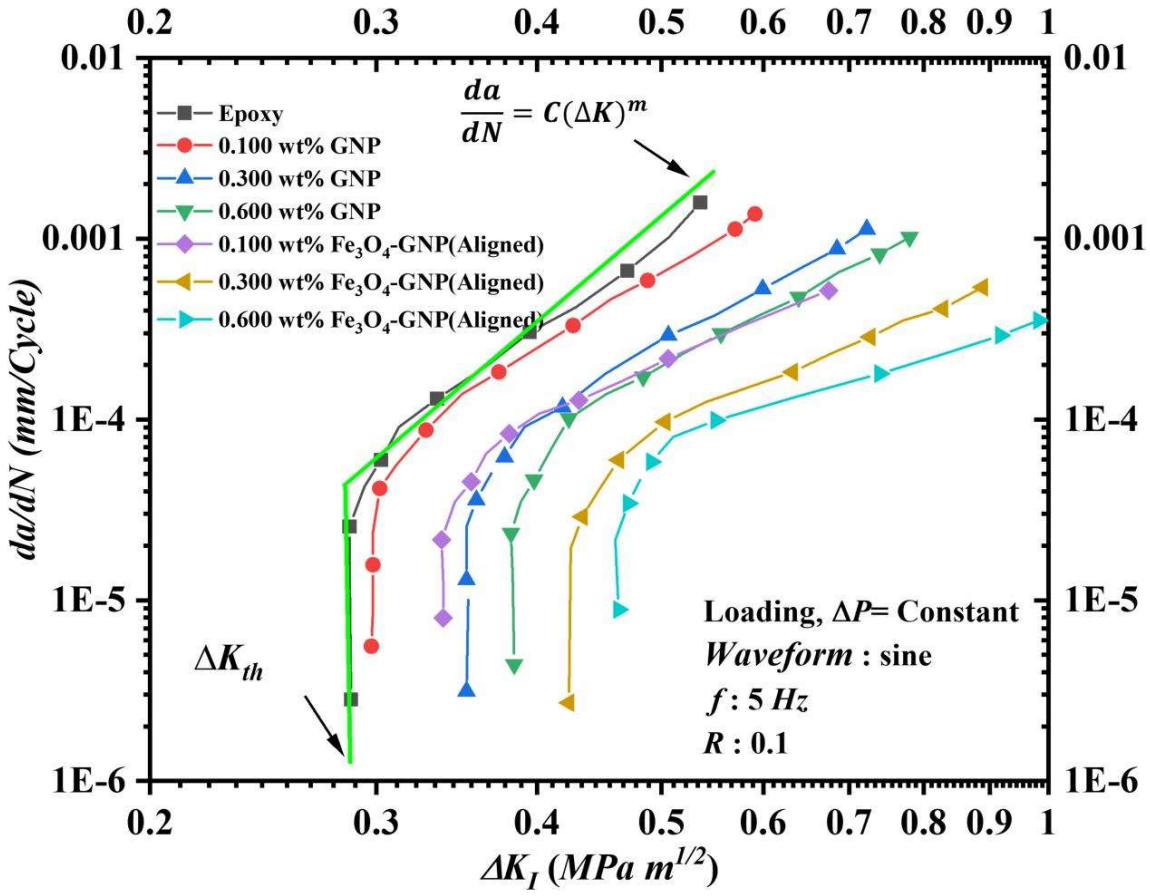

Fig. 6.7. Presents logarithmic plots (Log-Log) illustrating the correlation between the fatigue crack growth rate (da/dN) the stress intensity factor range (ΔK_I) specifically for epoxy, GNP epoxy, and aligned Fe_3O_4-GNP epoxy nanocomposites.

Furthermore, the constants *C*, *C'*, and *m* of the Paris Law have been determined through curve fitting and are provided in Table 6.1. Smaller values of these constants indicate a reduced rate of crack growth. Specifically, the Paris Law exponent has decreased from 7.14 for pure epoxy to 5.65 for epoxy nanocomposites with 0.600wt% GNP, and further down to 2.19 for epoxy nanocomposites with 0.600wt% aligned Fe_3O_4-GNP. These values closely align with previous

research findings for epoxy and GNP epoxy, suggesting that comparable resistance to fatigue crack propagation has been achieved at lower filler content in the nanocomposites.

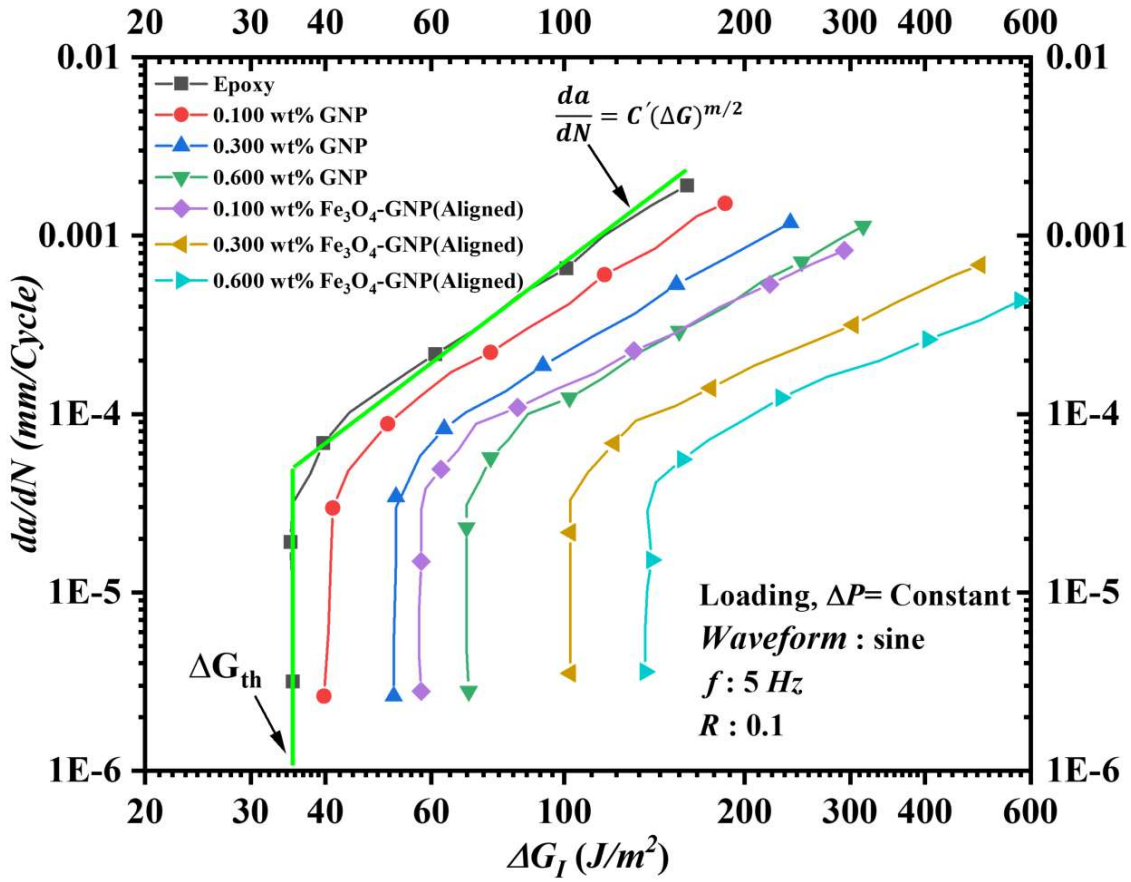

Fig. 6.8. Depicts logarithmic plots (Log-Log) illustrating the correlation between the fatigue crack growth rate (da/dN) and the strain energy release rate (ΔG_I) specifically for epoxy, GNP epoxy, and aligned Fe_3O_4-GNP epoxy nanocomposites

Moreover, the intercept value *C* has decreased from 1.73E-01 to 6.26E-3 for GNP epoxy, and to 3.55E-4 for aligned Fe_3O_4-GNP epoxy nanocomposites. Similarly, the intercept value *C′* has decreased from 8.87E-09 to 1.08E-8 for GNP epoxy, and to 2.98E-08 for aligned Fe_3O_4-GNP epoxy nanocomposites. A monotonic decrease in the Paris constants has been observed with an increasing weight percentage (wt%) of nanoparticles. Additionally, the constants have exhibited a significant decrease in the case of aligned Fe_3O_4-GNP, as compared to GNP epoxy and epoxy materials. These findings collectively demonstrate the effectiveness of GNP and aligned Fe_3O_4-GNP nanoparticles in impeding the growth of fatigue cracks in epoxy.

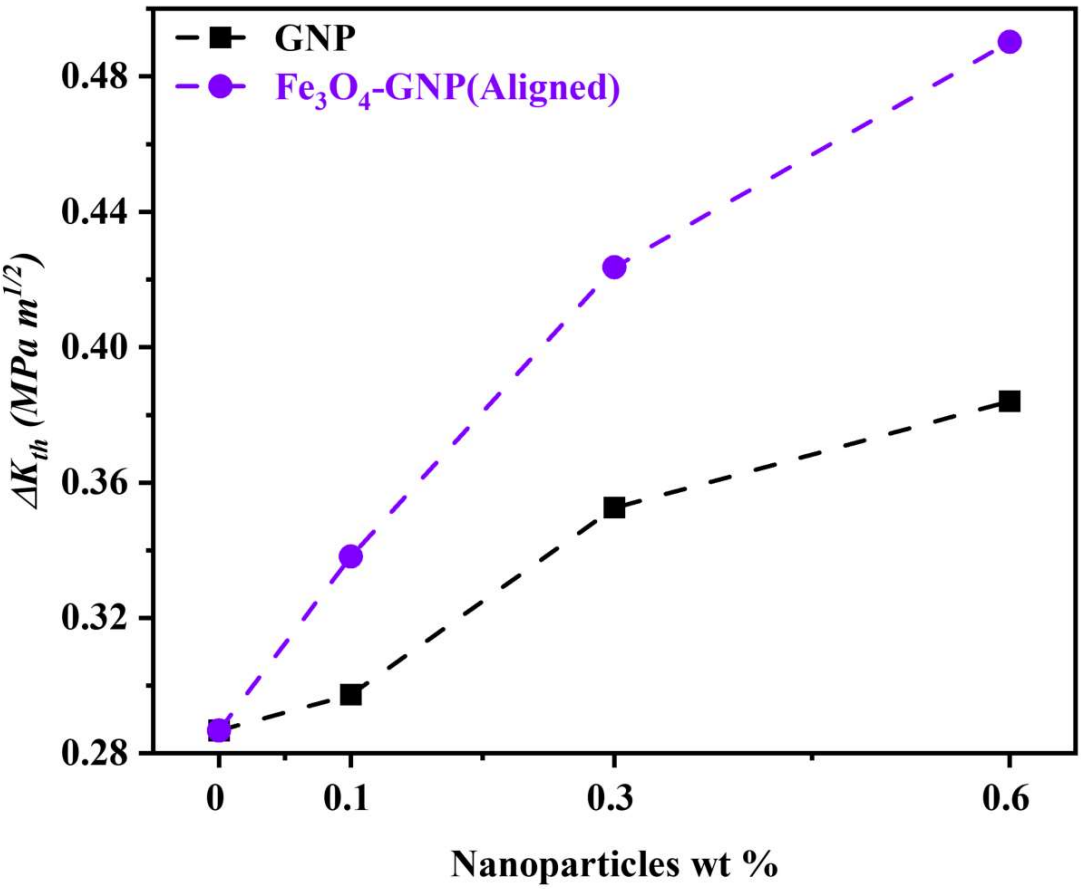

Fig. 6.9. Shows the influence of nanoparticles' wt% and the alignment of nanoparticles on the critical stress intensity factor (ΔK_{th}) specifically for epoxy, GNP epoxy, and aligned Fe_3O_4-GNP epoxy nanocomposites

Moreover, the notably smaller values of the Paris Law constants observed in aligned Fe_3O_4-GNP epoxy emphasize the enhanced effect of aligned Fe_3O_4-GNP nanoparticles compared to GNP nanoparticles. This highlights the significant role of aligned Fe_3O_4-GNP in further inhibiting fatigue crack growth and improving the fatigue resistance of the epoxy nanocomposites.

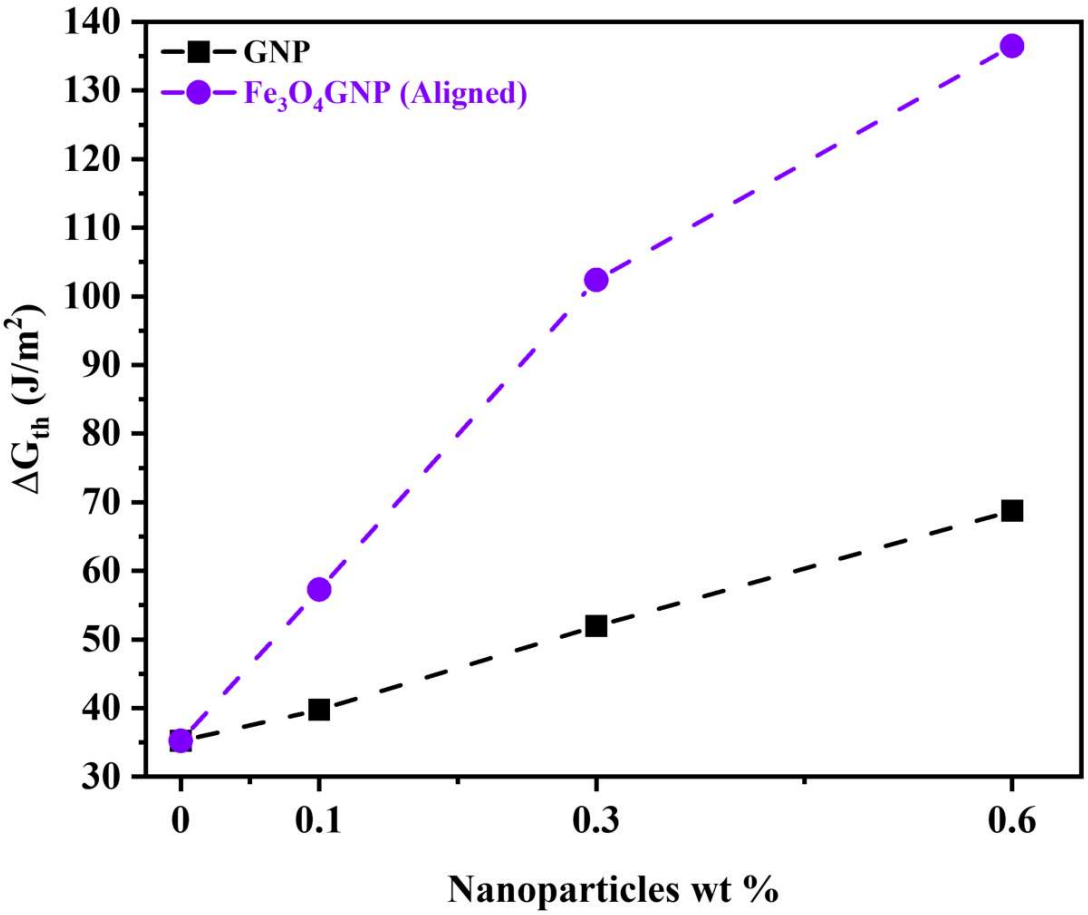

Fig. 6.10. Sows the influence of nanoparticles' wt% and the alignment of nanoparticles on the critical strain energy release rate (ΔG_{th}) specifically for epoxy, GNP epoxy, and aligned Fe_3O_4-GNP epoxy nanocomposites and

Table 6.1. The fatigue crack growth characteristics of epoxy, GNP epoxy, and aligned Fe_3O_4-GNP epoxy nanocomposites

	Fatigue crack growth threshold								Parameters for the Paris law					
	ΔK_{th} *(MPa $m^{1/2}$)*		$\Delta K_{th}/K_{IC}$		ΔG_{th} *(J/m^2)*		$\Delta G_{th}/G_{IC}$		*C (mm/cycle(MPa $m^{1/2}$)^m)*		*C′ (mm/cycle(J/m^2)$^{m/2}$)*		*m*	
wt%	**GNP (↑)**	Fe_3O_4-**GNP (↑)**	**GNP**	Fe_3O_4-**GNP**	**GNP (↑)**	Fe_3O_4-**GNP (↑)**	**GNP**	Fe_3O_4-**GNP**	**GNP**	Fe_3O_4-**GNP**	**GNP**	Fe_3O_4-**GNP**	**GNP**	Fe_3O_4-**GNP**
0.000	0.287 (0)	0.287 (0)	0.3050	0.3050	35.231 (0)	35.231 (0)	0.1685	0.1685	1.73E-01	1.73E-01	8.87E-09	8.87E-09	7.14	7.14
0.100	0.297 (3.70)	0.338 (17.94)	0.3097	0.3190	39.753 (12.84)	57.259 (62.53)	0.1760	0.2275	6.24E-02	2.63E-03	1.01E-08	7.47E-08	6.49	3.74
0.300	0.353 (22.96)	0.424 (47.75)	0.3176	0.3209	51.951 (47.46)	102.382 (190.60)	0.1970	0.3185	1.18E-02	7.91E-04	1.58E-08	3.87E-08	6.02	3.19
0.600	0.384 (33.94)	0.490 (70.98)	0.3200	0.3290	68.717 (95.05)	136.474 (287.37)	0.2280	0.3250	6.26E-03	3.55E-04	1.08E-08	2.98E-08	5.65	2.19

Note: - The ↑ denotes increments % values in the bracket.

6.3.5. Fatigue fracture surface analysis

The fractographic investigation of fatigue fracture surfaces have usually been initiated visually or through low-magnification optical microscopy. As a result of the change from an inclined stage I slip plane, which has been macroscopically perpendicular to the principal loading axis, one has often been able to distinguish a boundary between stage I and stage II crack propagations. In the analysis of stage changes, stereo zoom optical microscope images of the fatigue fracture surfaces of epoxy, GNP epoxy, and aligned Fe_3O_4-GNP of both 0.600wt% have been observed at three different stages: at the notch, near the pre-crack zone (stage I), at the center, representing stable crack growth zone (Stage II), and in the unstable crack zone where fracture occurs. The fatigue fracture surface analysis of epoxy, GNP epoxy, and aligned Fe_3O_4-GNP epoxy nanocomposites reveals that the crack initiation is observed to follow precisely with the razor-sharp pre-crack. Polymeric materials (epoxy) subjected to fatigue have frequently exhibited discontinuous crack propagation: the crack has been observed to occasionally stop and then resume propagation, sometimes with a sudden acceleration, after several cycles. In such cases, data readings have been taken as close as possible to crack arrest and re-start to ensure that the discontinuity is clearly apparent in a crack length (a) vs. elapsed cycles (N) plot[236]. These phenomena (marked with letter in circles on the images) are observed in the **Fig. 6.11** for the both nanocomposites. In the Fatigue fractured surface of the epoxy, after crack initiation, small striation marks with progressive crack bifurcation 'B', crack deflection 'C', and shear yielding straight 'S_y' have been observed. In the stable crack growth region, a slight crack tilting can be observed. However, overall, there have been mostly smooth regions between crack initiation and fracture points, with very few striation marks. All these features observed on the fatigue-fractured surfaces of the epoxy demonstrate the absence of any significant fatigue crack growth resistance phenomena. Additionally, they indicate that once

the applied stress intensity range ΔK_{IC} reaches its critical value ΔK_{th}, the crack propagates rapidly and in a straight manner until failure.

while the fatigue-fractured surfaces of GNP epoxy and Fe_3O_4-GNP epoxy have a number of fatigue crack growth resistance mechanisms due to the presence of the nanoparticle that makes the surfaces rougher than epoxy surfaces. from the figure, it can be observed that GNP epoxy and aligned Fe_3O_4-GNP epoxy have additional crack resistance mechanisms as compared to epoxy surfaces: Alteration of plane 'A', Local Mixed mode 'M', River line 'R', Twisting of crack 'T'. the presence of these mechanisms are frequently and more, which are more obstruct the crack growth and slow its growth rate. in these surfaces, we can easily observe the stage of crack growth with various mechanisms and roughness. In the epoxy, straight primary cracks can be seen once the crack starts propagating, and very less striation marks with coarser and spaced at a larger distance. while, in the GNP epoxy and aligned Fe_3O_4-GNP epoxy surfaces, primary cracks have multiple small secondary branches of crack which is the result of multiple above-discussed mechanisms Additionally also a debonding, pull out, cavitation, and delamination occurs at the microscopic level. However, the striation marks in the GNP epoxy and aligned Fe_3O_4-GNP epoxy are fine, closely spaced, and small in width, which indicates different crack growth behavior within these nanocomposites.

In light of the preceding discussions on fatigue fracture surfaces, the observation of fatigue fracture surfaces in the aligned Fe_3O_4-GNP epoxy is particularly intriguing. It is evident that these surfaces display a distinctive 3D plastic deformation of the matrix, characterized by deeper river lines and a heightened occurrence of associated mechanisms. This observation suggests that fatigue cracks in the aligned Fe_3O_4-GNP epoxy have developed in a discontinuous manner. Specifically, a localized zone of damage has formed at the crack tip in response to the applied K_{max}, and progressive damage has accumulated with each cycle at the prescribed ΔK_{IC} until reaching a critical crack-tip opening displacement. Subsequently, the crack has propagated

forward to the subsequent length of its equilibrium damage zone. This cyclic crack growth process continues, giving rise to discernible "sticks-slips" or fatigue striations.

The fatigue fracture surfaces of the GNP epoxy and aligned Fe_3O_4-GNP epoxy nanocomposite have revealed distinctive features, including deeper river lines, frequent occurrence of various mechanisms, well-defined and closely spaced striation marks, numerous small-sized rough patches, and the presence of strongly bonded nanoparticles that serve as effective pinning positions, inducing plastic deformation within the matrix during low crack propagation rates. These observations indicate enhanced crack closure and slowed crack propagation. Consequently, these mechanisms have effectively mitigated the FCGR of the nanocomposite, leading to a significant improvement in the fatigue life of the aligned Fe_3O_4-GNP-filled

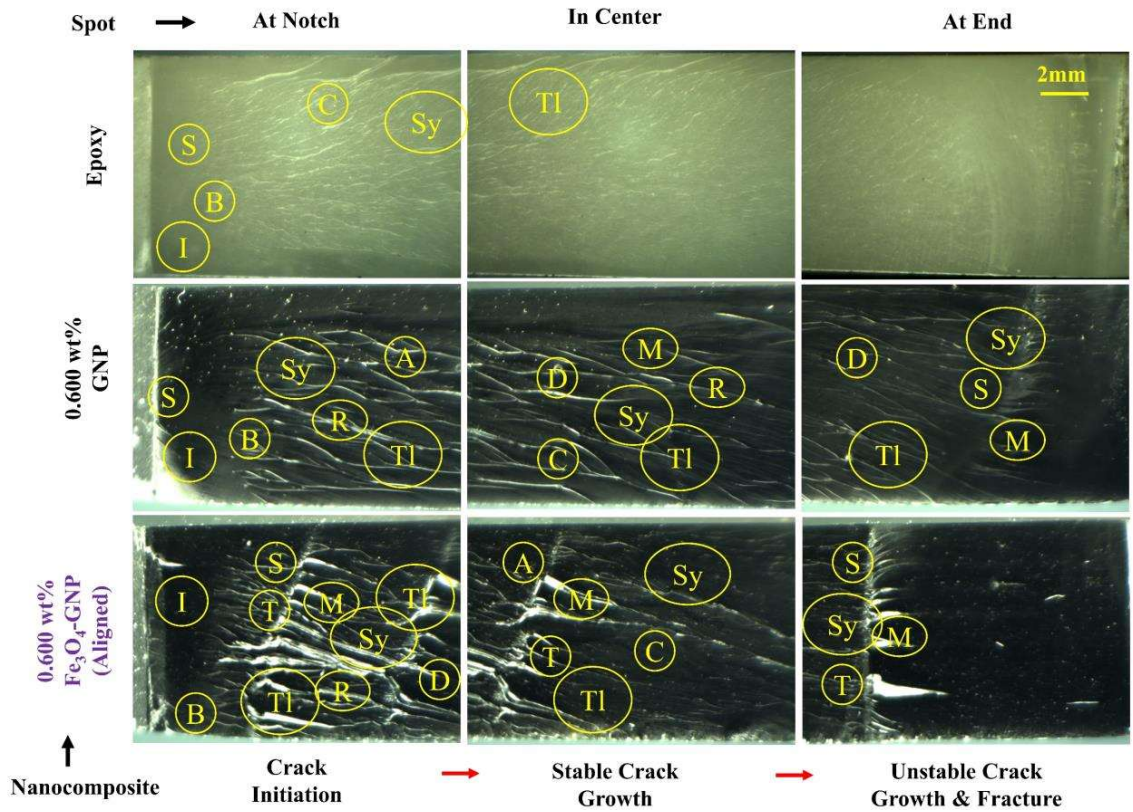

Fig. 6.11. Showcases stereo-zoom optical microscopic images of the fractured surfaces caused by the fatigue crack growth in epoxy, GNP epoxy, and aligned Fe3O4-GNP nanoparticle nanocomposites (0.600wt%) at three distinct progressive locations, illustrative of the mechanisms involved in the fatigue crack growth.(*Notion- A: Alteration of plane , B: Bifurcation, C: Crack deflection, D:, I: Initiation of crack, M: local Mixed mode, R: River line, T:Twisting, Tl: Tilting, S: Striation marks , Sy: Shear yielding.)*

nanocomposites when compared to those filled with random GNP or unfilled epoxy counterparts.

Fig. 6.12 shows 3D AFM images, waviness, and height profiles of fatigue fracture surfaces of epoxy, GNP epoxy, and aligned Fe_3O_4-GNP epoxy nanocomposites within a 20 x 20 μm area at the crack initiation site. Each surface exhibits distinct profiles, with the z-axis profile increasing with nanoparticle weight percentage and alignment. Nanoparticles in **Fig. 6.12 (b) and (c)** effectively impede the crack and align perpendicular to the crack growth direction, significantly enhancing the ΔK_{th} compared to epoxy and GNP epoxy. To understand fracture surface characteristics and mechanisms affecting fatigue crack growth resistance, specific roughness parameters are calculated for these materials. The calculated values are influenced by nanoparticle loading, increasing with higher weight percentage in the epoxy matrix and more sensitive alignments of Fe_3O_4-GNP (summarized in Table 6.2). Notably, Fe_3O_4-GNP alignment has a greater impact on roughness compared to nanoparticle loading (**Fig. 6.12 (c)**). Aligned Fe_3O_4-GNP nanocomposites exhibit significantly higher roughness values than GNP-reinforced composites. For instance, surface roughness (S_a) values for fatigue fracture surfaces are 3.26 nm, 7.10 nm, and 9.32 nm for epoxy, GNP epoxy, and aligned Fe_3O_4-GNP nanocomposites, respectively, indicating the substantial effect of alignment on surface morphology and fracture behavior. Neat epoxy has an RMS roughness (S_q) of 4.32 nm, while GNP and aligned Fe_3O_4-GNP nanocomposites have S_q values of 10.23 nm and 14.27 nm, respectively (Table 6.2). The alignment surpasses the S_q value of GNP nanocomposites by over 1.5 times. Additionally, the maximum height (S_z) values for neat epoxy, GNP, and aligned Fe_3O_4-GNP nanocomposites are 52.54 nm, 260.87 nm, and 663.34 nm, respectively. The area variation of the fracture surface for epoxy, GNP epoxy, and aligned Fe_3O_4-GNP epoxy is 11.03 μm^2, 45.30 μm^2, and 53.79 μm^2, respectively. The higher loading of GNP and aligned Fe_3O_4-GNP induces crack deflection, leading to increased peak and valley formations and larger fracture surfaces. Table 6.2 presents

volume parameters, integrating surface height over a 20 x 20 μm^2 area, and the variation in roughness computed as the integral of the local gradient, reflecting nanoparticle-induced roughness. These parameters suggest that nanoparticle reinforcement enhances ΔK_{th} and increases resistance to fatigue crack growth.

Fig. 6.12 (d) displays the waviness profile of the fatigue fracture surface, representing the path of crack growth. A notable observation has been made regarding the distinct crack paths of epoxy, GNP epoxy, and aligned Fe_3O_4-GNP nanocomposites. Specifically, a minimal height has been observed between the valley and peak, but with an increase in nanoparticle weight percentage, GNP and aligned Fe_3O_4-GNP have exhibited elevated heights. Notably, aligned Fe_3O_4-GNP nanocomposites have demonstrated a sudden jump in both the valley and peak regions. As a result, we have concluded that the sudden jump in the valley and peak of Aligned Fe_3O_4-GNP nanoparticles, combined with reinforcement, has increased the zig-zag nature of the crack growth path.

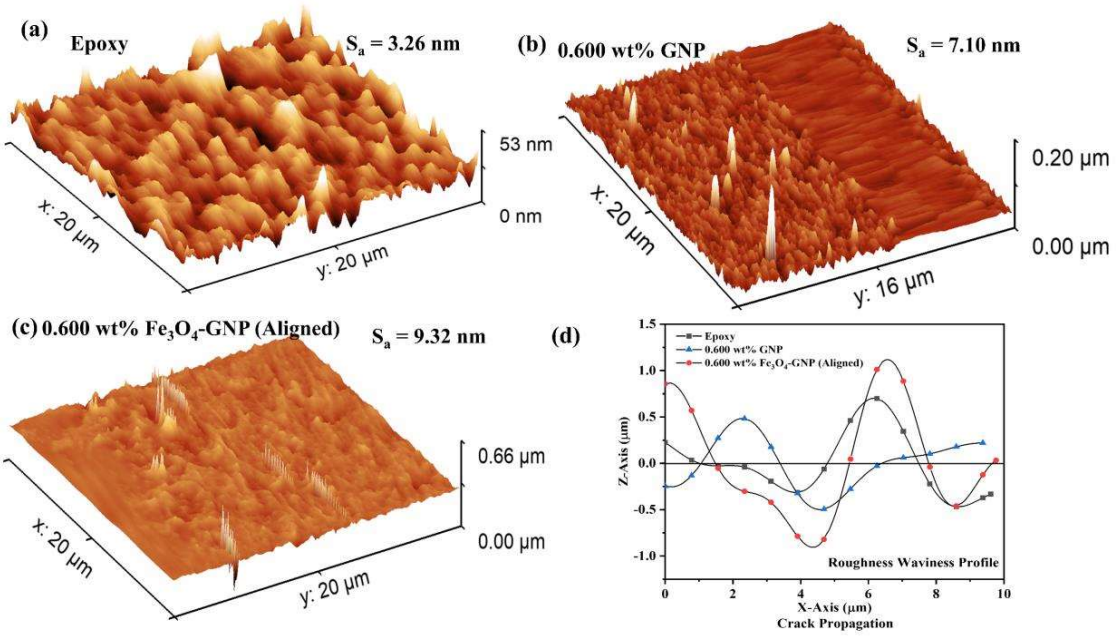

Fig. 6.12. Investigates the atomic force microscopy images of the fractured surfaces near the crack initiation in (a) epoxy, (b) GNP epoxy, and (c) aligned Fe_3O_4-GNP epoxy nanocomposites during fatigue crack growth. Notably, the images in (c) demonstrate the alignment of Fe3O4-GNP nanoparticles, while (d) exhibits the wavy characteristics of the fractured surfaces, resembling the path of the crack.

Table 6.2. The roughness parameters of fractured surfaces by Fatigue Crack Growth in epoxy, GNP epoxy, and aligned Fe_3O_4-GNP epoxy nanocomposites

wt%	RMS Roughness, S_q, (nm)	Maximum height, S_z, (nm)	Area Variation (µm^2)	Volume (µm^3)
Epoxy	4.32	52.54	11.03	8.825
GNP	10.23	260.87	45.3	20.731
Fe_3O_4-GNP	14.27	663.34	53.79	108.292

6.4. Discussion

In the earlier sections (6.2 and 6.3), we talked about how we set up the experiment, the steps we followed, and the specific results we obtained. We specifically discussed how the amount of nanoparticles used and the way Fe_3O_4-GNP particles are aligned had a big impact on the

nanocomposite material. However, we still need to analyze in more detail the reasons behind these outcomes and how they affect the properties of the nanocomposites. We are currently having ongoing discussions and investigations to gain a better overall understanding of the situation. In the ensuing section, a comprehensive examination of potential fatigue mechanisms shall be undertaken. These mechanisms encompass thermal softening[237–239], crack deflection[240–243], crack pinning [244–246], debonding[220,247], plastic void growth[248,249], and plastic deformation of the matrix. Each of these mechanisms shall be thoroughly explored and analyzed in the subsequent discussion.

6.4.1. Thermal softening

The interpretation and design of polymers (epoxy) under cyclic stress pose greater challenges compared to metals. Thermoplastics exhibit two distinct failure mechanisms: thermal softening and fatigue cracking. The extent of thermal softening is influenced by the damping, thermal conductivity and heat transfer coefficient of the material, which are impacted by factors such as reinforcement morphology, weight percentage, and distribution pattern in nanocomposites. The current specimen geometry effectively represents laboratory conditions, component proportions, and molding scenarios. Temperature rises calculations take into account variables like stress, frequency, heat transfer, surface area, volume, and density. Similar approximations are applied to actual components to determine the point of temperature stabilization and prevent thermal failure.

Under load-controlled cyclic fatigue loading, nanocomposites experience reduced modulus due to elevated temperature at the notch tip, increasing energy dissipation and leading to thermal failures. Efficient heat transfer mechanisms can prevent thermal softening by mitigating temperature rise[237]. Epoxy's high damping and low thermal conductivity hinder rapid heat transfer, making it more susceptible to thermal softening during fatigue[235]. In contrast, GNP have excellent thermal conductivity, enhancing the overall thermal conductivity of GNP epoxy

nanocomposites[45]. This enables swift transfer of cyclically generated heat, resulting in significant fatigue life improvement across all load levels. Incorporating aligned Fe_3O_4-GNP further enhances thermal conductivity and reduces damping characteristics. The strategic alignment of Fe_3O_4-GNP perpendicular to crack growth imparts superior properties to aligned Fe_3O_4-GNP epoxy nanocomposites, surpassing epoxy, and GNP epoxy nanocomposites. In summary, the inclusion of GNP and aligned Fe_3O_4-GNP not only mitigates temperature elevation but also slightly prolongs the failure process. GNP epoxy and aligned Fe_3O_4-GNP nanocomposites exhibit lower temperatures and effective heat dissipation, successfully averting thermal softening[239].

6.4.2. Fatigue crack growth mechanism

To investigate the mechanism of crack growth in the epoxy resin composite under consideration, a more detailed in situ observation of the crack tip was conducted. An example of such observation is presented in **Fig. 6.11** , which reveals the presence of micro-cracks at the crack tip. The fatigue fracture surface of epoxy has exhibited a lower frequency of micro-cracks compared to GNP epoxy and aligned Fe_3O_4-GNP epoxy. However, the presence of micro-cracks on the fatigue fracture surface of aligned Fe_3O_4-GNP epoxy has been significantly greater in comparison to epoxy and GNP epoxy. Over several cycles, these micro-cracks merge together, forming a primary crack. Subsequently, new micro-cracks develop at the tip of the merged primary crack. These newly formed micro-cracks then combine to create another primary crack. The occurrence of micro-cracking predominantly transpires at the interface between the epoxy matrix and either GNP or Fe_3O_4-GNP. The nanoparticles utilized in this study are characterized by irregular shapes and have undergone crushing, resulting in high stress concentration at the interface and facilitating the initiation of micro-cracks.

A comprehensive AFM was conducted to examine the fracture surface characteristics **Fig. 6.12**. The obtained data (summarized in Table 6.2) revealed a notable increase (S_q: 4.32 nm to 14.27

nm) in the average surface roughness when the GNP and aligned Fe_3O_4-GNP content was increased from 0 to 0.600 wt.%. This rise in roughness facilitated crack deflection, thereby leading to an augmented total fracture surface area (11.03 μm^2 to 53.79 μm^2) in the epoxy, GNP epoxy and aligned Fe_3O_4-GNP epoxy nanocomposite. Additionally, the presence of tilting and twisting in the crack front necessitated localized crack growth under mixed mode conditions, demanding a higher level of driving force compared to Mode I conditions. The rough fracture surfaces of the nanocomposite have indicated a higher consumption of energy during fatigue crack advancement. The reinforcement of GNP and aligned Fe_3O_4-GNP has delayed the fatigue failure by impeding the crack growth rate. The resistance to FCGR has been higher with aligned Fe_3O_4-GNP epoxy nanocomposites as nano reinforcement than that of GNP. The formation of river marks, as shown in **Fig. 6.11**, can be attributed to the formation of shear bands preceding the crack tip[250]. Notably, the fractured surface of 0.600wt% GNP epoxy and aligned Fe_3O_4-GNP nanocomposites exhibited wider river marks. Furthermore, secondary short river marks were observed at select locations, both at the center and towards the end.

In **Fig. 6.11**, various features on the fractured surfaces have been identified and labeled with different letters of the alphabet. These features include crack bifurcation, crack bifurcation and crack plane shift, crack bowing, matrix spalling, deep craters, and secondary striation. The presence of secondary river marks, crack deflection, and microcracking indicates a higher consumption of energy, leading to a delay in the rate of FCGR in the nanocomposite[251]. In the case of GNP and aligned Fe_3O_4-GNP epoxy nanocomposites, the formation of shear bands appears to be the primary mechanism responsible for the elevated resistance to FCGR [252].

Neat epoxy's crack tip was characterized without detecting damage mechanisms, similar to brittle-like polymers. Adding GNP and aligned Fe_3O_4-GNP nanoparticles changes the fracture process, creating a tortuous crack path (**Fig. 6.11**). Aligned Fe_3O_4-GNP composites show greater deviations, leading to significant advancements. Optical images aid in observing crack

propagation and growth behavior. Stress concentrations at epoxy-nanoparticle interfaces, caused by modulus and Poisson's ratio mismatch, lead to microcracks via delamination and debonding.

Fig. 6.12 (a) to (c), indicates higher surface roughness in nanocomposites with increased GNP and aligned Fe_3O_4-GNP, improving toughness (also summarized in Table 6.2). Alignment of Fe_3O_4-GNP increases crack deflection and branching, enhancing toughening. The ongoing discussion on toughening mechanisms in nanoparticle-reinforced epoxies acknowledges the importance of debonding, cavitation, void expansion, matrix shear deformation, crack deflection, twisting, and bridging for energy dissipation and fracture resistance. Extensive literature studies, including references[190,216–221] , have explored the multifaceted fracture behavior of nanoparticle-reinforced resins crucial to engineering applications.

Crack pinning occurs when a crack encounters nanoparticles, causing bow-shaped deformation seen in waviness profiles (**Fig. 6.12 (d)**). Nanoparticle type and orientation influence crack front deformation. Aligned Fe_3O_4-GNP exhibits higher amplitude. Fracture surface examination and roughness parameters (Table 6.2) confirm aligned Fe_3O_4-GNP's superior resistance to crack propagation.

AFM demonstrate pulled-out GNP and aligned Fe_3O_4-GNP nanoparticles, indicating crack face bridging under mode-I fatigue crack growth. Jagged edges enhance fatigue crack growth resistance and resist pull-out forces via mechanical lock (**Fig. 6.12**). Nanoparticles shift the fatigue crack growth from plane strain to plane stress condition, inducing shear yielding[7,222]. Voids, cavities, and debonding at the crack tip contribute to this change. Nanoparticles act as local constraints, transitioning from 2D to 3D strains, increasing plastic deformation near the crack front [223]. These enhance ΔK_{th} (orΔG_{th}) and fatigue crack growth, with aligned Fe_3O_4-GNP at 0.600wt% load achieving the highest ΔK_{th} enhancement.

6.5.Conclusion

The present study comprehensively explores the ΔK_{th} (orΔG_{th}) and fatigue crack growth resistance of epoxy, GNP epoxy, and aligned Fe_3O_4-GNP epoxy nanocomposite. Aligned Fe_3O_4-GNP nanoparticles have resulted in a more significant improvement in ΔK_{th} ,ΔG_{th} , and resistance to fatigue crack growth by reducing thermal softening and enhancing the fatigue crack growth mechanism compared to GNP reinforcement epoxy alone. This suggests the potential of aligned Fe_3O_4-GNP reinforced epoxy nanocomposites as superior materials for engineering applications.

This page intentionally left blank